

AperTO - Archivio Istituzionale Open Access dell'Università di Torino

## Thermoelastic behavior and dehydration process of cancrinite

### This is the author's manuscript

*Original Citation:*

*Availability:*

This version is available <http://hdl.handle.net/2318/142918> since

*Published version:*

DOI:10.1007/s00269-014-0656-2

*Terms of use:*

Open Access

Anyone can freely access the full text of works made available as "Open Access". Works made available under a Creative Commons license can be used according to the terms and conditions of said license. Use of all other works requires consent of the right holder (author or publisher) if not exempted from copyright protection by the applicable law.

(Article begins on next page)



# UNIVERSITÀ DEGLI STUDI DI TORINO

***This is an author version of the contribution published on:***

*Questa è la versione dell'autore dell'opera:*

*Physics and Chemistry of Minerals*, 41, 5, 2014, <http://dx.doi.org/10.1007/s00269-014-0656-2> ]

***The definitive version is available at:***

*La versione definitiva è disponibile alla URL:*

[link.springer.com](http://link.springer.com)

# **THERMOELASTIC BEHAVIOR AND DEHYDRATION PROCESS OF CANCRINITE**

**Running title:** HT behavior of cancrinite

**Abstract**

**Introduction**

**Experimental methods**

- *Sample preparation*
- *Calibration of the furnace*
- *Unit-cell parameters and intensity data collections*
- *Thermal Equation of State*
- *Structure refinements*

**Results and discussion**

- *Unit-cell parameters evolution with  $T$*
- *High-temperature structural evolution and the effects of the dehydration process*
- *Comparison with previous studies*

**Acknowledgements**

**References**

**Figures/Tables**

**Corresponding author: G. Diego GATTA**

Dipartimento di Scienza della Terra  
Universita' degli Studi di Milano  
Via Botticelli, 23  
I-20133 Milano, Italy  
Tel. +39 02 503 15607  
Fax +39 02 503 15597  
E-Mail: [diego.gatta@unimi.it](mailto:diego.gatta@unimi.it)

Operating system: Windows XP

# THERMOELASTIC BEHAVIOR AND DEHYDRATION PROCESS OF CANCRINITE

G.D. Gatta<sup>1,2</sup>, D. Comboni<sup>3</sup>, M. Alvaro<sup>4</sup>, P. Lotti<sup>1</sup>, F. Cámara<sup>5,6</sup>, M.C. Domeneghetti<sup>3</sup>

<sup>1</sup>Dipartimento di Scienze della Terra, Università degli Studi di Milano, Via Botticelli 23, I-20133 Milano, Italy

<sup>2</sup>CNR - Istituto di Cristallografia, Sede di Bari, Via G. Amendola 122/o, Bari, Italy

<sup>3</sup>Dipartimento di Scienze della Terra e dell'Ambiente, Università di Pavia, Via Ferrata 1, I-27100 Pavia, Italy

<sup>4</sup>Dipartimento di Geoscienze, Università degli Studi di Padova, Via Gradenigo, 6, I-35131 Padova, Italy

<sup>5</sup>Dipartimento di Scienze della Terra, Università degli Studi di Torino, via Valperga Caluso 35, I-10125 Torino, Italy

<sup>6</sup>CrisDi, Interdepartmental Centre for the Research and Development of Crystallography, Torino, Italy

## ABSTRACT

The high-temperature thermo-elastic behavior of a natural cancrinite has been investigated by *in-situ* single-crystal X-ray diffraction. The unit-cell volume variation as a function of temperature ( $T$ ) exhibits a continuous trend up to 748 K (hydrous expansion regime). The unit-cell edges expansion clearly shows an anisotropic expansion scheme ( $\alpha_a < \alpha_c$ ). At 748 K, a dehydration process takes place and a series of unit-cell parameters measurements at constant temperature (748 K) for a period of 12 days indicates that the dehydration process continued for the entire period of time, until the cell parameters were found to be constant. After the dehydration process is completed, the structure expands almost linearly with increasing temperature up to 823 K, where a sudden broadening of the diffraction peaks, likely due to the impending decomposition, did not allow the collection of further data points. Even with a very limited temperature range for the anhydrous regime, we observed that the behavior of the two (*i.e.*, hydrous and anhydrous) high-temperature structures is similar in terms of (i) volume thermal expansion coefficient and (ii) thermo-elastic anisotropy.

The structure refinements collected at 303, 478 and 748 K (after the dehydration), respectively, showed a change in the mechanism of tilting of the quasi-rigid (Si,Al)O<sub>4</sub> tetrahedra, following the loss of H<sub>2</sub>O molecules, ascribable to the high-temperature Na<sup>+</sup> coordination environment within the cages.

**KEYWORDS:** Cancrinite, thermal expansion, single-crystal X-ray diffraction, dehydration.

## INTRODUCTION

Cancrinite is a microporous silicate with ideal chemical formula

$[(\text{Na,Ca})_{5-6}(\text{CO}_3)_{1.4-1.7}][\text{Na}_2(\text{H}_2\text{O})_2][\text{Al}_6\text{Si}_6\text{O}_{24}]$  (Bonaccorsi and Merlino 2005) and belongs to the homonymous group of minerals. Cancrinite usually occurs as (i) a primary phase in intrusive low SiO<sub>2</sub> alkali-rich rocks in the late hydrothermal stages; (ii) as alteration product from nepheline or sodalite-group minerals (Bonaccorsi and Merlino 2005; Pekov et al. 2011; Cámara et al. 2005; Lotti et al. 2012 ). The structure consists of an open framework of tetrahedra (framework density =  $16.9 \text{ T}/10^3 \text{ \AA}^3$ , Gatta et al. 2012), made of 12-, 6-, 4-

membered rings of TO<sub>4</sub> tetrahedra, where T site is occupied by Si and Al. These rings are arranged in such a way that planes of single six-membered rings perpendicular to the [0001] axis ( $S6R \perp [0001]$ ) are stacked according to an ...A-B-A-B-... close packing sequence (Figure 1). The resulting framework consists of (i) columns of base-sharing cages (*can* unit, undecahedral cage or  $\epsilon$ -cage) and (ii) iso-oriented twelve-membered ring (12mR) channels parallel to the [0001] axis (Figure 1). The *can* units (cages) and the channels are connected by

distorted S6R-windows approximately parallel to [0001] ( $S6R \angle [0001]$ ) (Figure 1). The single four rings (S4R) form double *zigzag* chains of tetrahedra running parallel to [0001] (Figure 1). The *can* units host  $[Na \cdot H_2O]^+$  chains, while the large channels are occupied by  $Na^+$ ,  $Ca^{2+}$  and  $[CO_3]^{2-}$  groups. Each  $H_2O$  molecule forming the  $[Na \cdot H_2O]^+$  chain has one of the two  $Na-OH_2$  bonds stronger than the other (Figure 2). The resulting chain is therefore a sequence  $-H_2O(I)-Na(I)-H_2O(II)-Na(II)-$  where the average bond distance of the stronger bond ( $\langle H_2O(I)-Na(I) \rangle$ ) is 2.3412 Å while the one of the weaker bond ( $\langle H_2O(II)-Na(I) \rangle$ ) is

2.8925 Å (Grundy and Hassan 1982; Hassan and Grundy 1991, Isupova et al. 2010; Della Ventura et al. 2009; Gatta et al. 2012; Lotti et al. 2012). The 12mR-channels host cations (*i.e.*,  $Na^+$ ,  $Ca^{2+}$  and rarely  $K^+$ ) near the walls and  $[CO_3]^{2-}$  anionic groups in the center in two mutually exclusive positions (Figure 2). The 12mR-channels can host several anionic complexes such as  $NO_3^-$ ,  $Cl^-$ ,  $OH^-$ ,  $CO_3^{2-}$  or even chains, *e.g.* chains of  $Se_2^{2-}$  and  $Se_2^-$  that provide interesting optical properties (Poborchii 1994; Poborchii et al. 2002).

Several studies have been devoted to the cancrinite behavior at non-ambient conditions. Hassan (1996a) studied the high-*T* elastic behavior of cancrinite by means of X-ray powder diffraction (PD-XRD) in a range of temperatures from 293 to 1673 K, where the decomposition clearly takes place. Hassan (1996b) reported also a description for the  $H_2O$  and  $CO_2$  loss processes, as a function of temperature, by thermogravimetric (TG) and differential thermal analysis (DTA). A further study (Sirbescu and Jenkins 1999) was performed on the synthesis and upper thermal stability of cancrinite, investigated experimentally in the system  $Na_2O-CaO-Al_2O_3-SiO_2-CO_2-H_2O$ , demonstrating the important

role that water plays in controlling the stability of cancrinite in igneous and metamorphic rocks. Later, Hassan et al. (2006) performed an *in-situ* high- $T$  synchrotron powder diffraction experiment on cancrinite aimed to determine the elastic behavior and the H<sub>2</sub>O loss with increasing  $T$ . For their experiments, Hassan et al. (2006) used a natural cancrinite, which exhibited superstructure reflections. The authors reported the breakdown of the superstructure along [0001], with a sharp discontinuity in the unit-cell parameters at 777 K, along with a continuous loss of H<sub>2</sub>O up to 898 K, where an anhydrous phase is reported up to 1225 K. A TG- and DTA-study of a synthetic (NO<sub>3</sub>)-cancrinite was also performed by Fechtelkord et al. (2001), who reported a three-stage loss pattern, interpreted as follows: a first stage (*i.e.*, 296-400 K) with release of surface water, a second stage (*i.e.*, 450-600 K) with loss of cage-H<sub>2</sub>O, and a third stage (*i.e.*, 800-1000 K) assigned to the decomposition of the framework and enclathrated nitrate. A single-crystal high- $T$  X-ray diffraction study of cancrinite was performed by Isupova et al. (2010), in order to investigate the asymmetric probability density function of the atomic sites, for the calculation of the pyroelectric coefficients. Recently, Lotti et al. (2012, 2014) investigated the high-pressure behavior of cancrinite and balliranoite by *in-situ* single-crystal X-ray diffraction (SC-XRD) under hydrostatic conditions up to about 7 GPa. For the experiment on cancrinite, Lotti et al. (2012) used a fragment from the same gem-quality sample from Cameroun previously used by Della Ventura et al. (2009) for single-crystal FTIR and neutron diffraction experiments. A single-crystal from the same sample was also studied at low temperature ( $T \leq 293$  K) by *in-situ* X-ray diffraction (Gatta et al. 2012). Gatta et al. (2012) and Lotti et al. (2012) reported the low- $T$  and high- $P$  thermo-elastic behavior of cancrinite and its low- $T$ - and  $P$ -induced structural evolution, with a description of the main deformation mechanisms, which turned to be similar though with a different magnitude. Very recently, Kurdakova et al. (2013) have performed a study on the

thermodynamic properties of synthetic calcium-free cancrinite, reporting new values of the heat capacity, third-law absolute entropy, enthalpy and Gibbs free energy of formation.

Despite several studies were devoted to cancrinite at high temperature (Hassan 1996a, 1996b; Sirbescu and Jenkins 1999; Fechtelkord et al. 2001; Hassan et al. 2006; Isupova et al. 2010), a clear picture of its behavior is still missing. In particular, an unambiguous description of the dehydration process and of the  $T$ -induced deformation mechanisms, at the atomic level, is lacking. In addition, some of the previous results appear to be conflicting. In this light, the aim of this study is to investigate the thermal expansion behavior and the dehydration mechanism of cancrinite by *in-situ* single-crystal X-ray diffraction. A series of high- $T$  unit-cell edges measurements and intensity data collections were performed, in order to provide a clearer picture of the cancrinite behavior, at atomic level, in response to the applied temperature.

## EXPERIMENTAL METHODS

### - *Sample preparation*

The *in-situ* high-temperature X-ray diffraction experiment was performed on a crystal fragment (size 300 x 200 x 150  $\mu\text{m}^3$ ), from the main batch already used by Della Ventura et al. (2009), Gatta et al. (2012) and Lotti et al. (2012), showing sharp optical extinction with crossed polarized light under the microscope. The previous diffraction studies reported no superstructure reflections. The crystal was mounted inside a 0.3 mm inner diameter and 26 mm long quartz capillary (kept open), and was held in place by quartz wool to avoid any mechanical stress. The capillary was mounted on a metal goniometer head on the Philips PW1100 diffractometer ( $\text{MoK}\alpha$  radiation), working at 30 mA/50 kV and using a 0.5 mm pinhole short collimator, operated with FEBO software (a local developed control software).

On top was placed a microfurnace (controlled by a Eurotherm unit) with an H-shaped Pt–Rh resistance and a Pt:Pt–Rh thermocouple inside a steel cylindrical cage 1 inch wide closed with a Kapton film (*e.g.*, Redhammer et al. 2010, Alvaro et al. 2011).

- *Calibration of the furnace*

Due to the low thermal conductivity of quartz and the distance between the thermocouple tip and the crystal inside the quartz vial (ca. 1.5 mm), the reading of the controller is not the actual temperature of the crystal. To overcome this problem, a temperature calibration was undertaken by: (i) observing the melting of selected pure salts, (ii) measuring the thermal expansion of quartz across the  $\alpha - \beta$  phase transition. A spherical crystal of quartz was mounted on a quartz vial. Unit-cell parameters were collected at high temperature every 25 K. Linear fitting, performed on the observed melting points and on the observed  $\alpha - \beta$  transition temperature of quartz vs. the recorded temperature at the controller display, yielded the following equation:

$$T = 8.852(4.353) + 1.153(9) * T_{\text{display}}$$

with  $\pm 1$  K on the reading of the thermocouple. Gaussian error propagation yielded a 6.75 K  $1\sigma$  error at room- $T$  and 7.04 K at 973 K. The temperature stability of the furnace while changing goniometer position was within a few K.

- *Unit-cell parameters and intensity data collections*

Unit-cell parameters (Tables 1 and 2, Figure 3) were refined using the Philips URF and LAT routines, by least-squares refinement of the UB-matrix on the basis of 24 and 60 selected intense reflections, respectively, in the  $\theta$ -range 2-34° (Redhammer et al. 2010, Alvaro et al. 2011, Ferrari et al. 2014). Data were collected at intervals of 25 K in the  $T$  range 293-823 K. The UB matrix, and so the unit-cell parameters, were firstly refined by measuring

the Bragg angles of the selected 24 most intense reflections, using horizontal and vertical slits. Afterward, the Philips LAT routine was used to obtain accurate and precise unit-cell parameters. The LAT routine allowed the position of different reflections (with different  $nd$ -values, where  $d$  is the interplanar distance and  $n = 1, 2, 3, 4, \dots$ ), at positive and negative  $\omega$ - $2\theta$ , to be measured. The reflection is firstly centered by using the vertical and horizontal slits, then a scan in  $\omega$ - $2\theta$  is performed and the observed maxima are determined. The observed  $nd$ -values were fitted producing a relative  $d$ -value and its e.s.d.'s. The procedure was repeated for each temperature step on a group of 60 reflections, and lattice parameters were calculated by least-squares fitting of all the observed  $d$ -values.

The protocol applied at each temperature step consists in a small set of URF procedures (approx 10 minutes each) aimed to the refinement of the UB matrix until the complete relaxation is reached (*i.e.*, when the difference between the observed position for the 24 peaks in two subsequent measures are negligible). Only when the unit-cell parameters did not change anymore, the LAT procedure was performed. The results of the aforementioned protocol for the unit-cell edges measurements at each temperature step are reported in Tables 1 and 2 and in Figure 3. At 748 K, the unit-cell parameters achieved the relaxation only after 12 days. The isothermal data at 748 K are reported in Figure 4.

Intensity data collections were performed at 303, 448, and 748 K, respectively. Profiles of  $2.1^\circ$  in  $\omega$  at fixed scan rate of  $0.07^\circ\text{sec}^{-1}$  were integrated using the Lehmann and Larsen (1974) approach, and the integrated intensities were then corrected for Lorenz-polarization and absorption effects using a  $\psi$ -scan method (North et al. 1968).

#### - *Thermal Equation of State*

In order to describe the thermo-elastic behavior of cancrinite, the unit-cell volume with  $T$  could be easily fitted to the equation proposed by Gottschalk (1997):

$$V(T) = V_{0(P_r, T_r)} \exp[\alpha_r(T - T_r)] \quad (1)$$

where  $V_0$ ,  $P_r$  and  $T_r$  are the reference volume, pressure and temperature, respectively. However, this equation assumes the thermal expansion coefficient ( $\alpha_V = 1/V(\partial V/\partial T)$ ) to be completely independent from temperature. Therefore, in order to account for  $\alpha$  variations with  $T$ , the fit of the unit-cell parameters trend with  $T$  was performed with a modified second-order polynomial equation proposed by Berman (1988), using the EoSFit software (courtesy of Ross J. Angel), as follows:

$$V(T) = V_{0(P_r, T_r)} \exp[a_0(T - T_r) + \frac{1}{2} \cdot a_1(T^2 - T_r^2)] \quad (2)$$

where  $V_0$ ,  $P_r$  and  $T_r$  are the reference volume, pressure and temperature, respectively, and the thermal expansion coefficient described as:  $\alpha_{V, T_r} = a_0 + a_1(T - T_r)$ . In addition, in order to account for  $\alpha$  saturation at high- $T$ , a further fit was performed using a modified version of the equation proposed by Pawley et al. (1996) and Holland and Powell (1998), rewritten as:

$$V(T) = V_{0(P_r, T_r)} [1 + a_0(T - T_r) - 2 \cdot (10a_0 + a_1)(\sqrt{T} - \sqrt{T_r})] \quad (3)$$

where  $V_0$ ,  $P_r$  and  $T_r$  are the reference volume, pressure and temperature, respectively, and the thermal expansion coefficient modeled as:  $\alpha_{V, T_r} = a_0 - [(10a_0 + a_1)/\sqrt{T}]$  (see the manual of the EoSFit software at <http://www.rossangel.com/> for further details). Even considering the small range of temperature investigated, all the volume-temperature data (Table 1) were fitted with the two abovementioned empirical equations (*i.e.*, Berman 1988; Pawley et al. 1996) in order to select the best representative fitting model for our dataset (Table 6).

- *Structure refinements*

Structure refinements have been performed from the intensity data collected at 303, 448 and 748 K, in the space group  $P6_3$  (as suggested by the systematic extinctions) using the SHELXL-97 software (Sheldrick 1997, 2008) implemented in the WinGX suite of crystallographic programs (Farrugia 1999). Neutral X-ray scattering factors for Si, Al, Na, Ca, C and O were taken from the *International Tables of Crystallography, Vol. C* (Wilson and Prince 1999). The structure of cancrinite at 303 K was refined starting from the framework coordinates of Della Ventura et al. (2009), and localizing the extraframework population by difference-Fourier syntheses of the electron density maps. In order to get a stable refinement, some restraints were applied: i) the Na<sub>2</sub>/Ca<sub>2</sub> site was refined applying a mixed Na/Ca X-ray scattering curve and constraining their fractions to sum full occupancy (a test refinement with occupancy factors free to vary validated this as a good approximation, *i.e.* within  $2\sigma$ ); ii) the C1-OC1 and C2-OC2 bond distances were restrained to 1.300(5) Å following a previously reported procedure (Gatta et al. 2012; Lotti et al. 2012); iii) the C1-C2 and OC1-OC2 sites were constrained to share the same displacement parameters ( $dp$ 's), respectively. Convergence was achieved in the last cycles of refinement with anisotropic  $dp$ 's for all the sites, excluding Ow. Constraining C1-C2 and OC1-OC2, respectively, to share the same anisotropic  $dp$  was considered an acceptable compromise, as the  $dp$ 's of these sites are mainly influenced by the positional disorder along [0001], which equally involves the C1-OC1 and C2-OC2 groups as shown by the difference-Fourier maps in Figure 5. The structure refinement based on the 448 K dataset was performed constraining the Na and Ca fractions of the Na<sub>2</sub>/Ca<sub>2</sub> site to the values refined at 303 K and restraining the C1-C2 and OC1-OC2  $dp$ 's to an isotropic function. A test refinement with the Ow occupancy factor ( $sof$ ) free to vary suggested a full occupancy. The 748 K structure refinement was carried out with the same strategy, but refining the  $sof$ (Ow) and constraining its  $dp$  to the value refined at 478 K, for

which a detailed discussion is given later. All the refinements converged with no significant residues in the difference-Fourier syntheses and no significant correlation between the refined parameters. Further details pertaining to the structure refinements are given in Table 3. Atomic site coordinates, occupancy factors and equivalent/isotropic  $dp$ 's are in Table 4; relevant bond distances, angles and structural parameters in Table 5. Anisotropic displacement parameters are deposited (Table 4dep).

## RESULTS AND DISCUSSION

### - *Unit-cell parameters evolution with $T$*

The unit-cell parameters evolution with  $T$  (Tables 1 and 2, Figures 3 and 4) shows three different expansion regimes: (i) the first trend, for the hydrated structure, from room- $T$  (291 K) to 748 K, where all the unit-cell parameters ( $a$ ,  $c$ ,  $V$ ) expand almost linearly with increasing  $T$  (Figure 3); (ii) the dehydration regime (748 K), where a contraction of all the unit-cell parameters takes place (Figures 3 and 4); (iii) the second expansion regime, from 748 K to 823 K, where the quasi-dehydrated structure expands upon increasing  $T$  (Figure 3). A discussion about the quasi-dehydrated form is given below.

In order to test the quality of the fitting protocols (Table 6), in terms of difference between the unit-cell volume calculated from the thermal-equations fit and the actual measured volume, the  $\delta V$  parameter, defined as the difference between observed and calculated volume, was calculated at different  $T$  (Figure 6). The  $\delta V$  clearly shows that both the modified equations of Pawley et al. (1996) and Berman (1988) reproduce very well the thermal expansion behavior within the entire hydrous expansion regime (from room- $T$  to 748 K), with the exception of the last data points due to the impending dehydration (at 748 K) (arrows in Figure 6).

While the limited range of temperature investigated for the quasi-anhydrous thermal expansion regime (*i.e.*, 748K – 823K) allowed a good quality fit adopting the modified equation by Berman (1988), a low-quality was obtained with the modified equation by Pawley et al. (1996). For the sake of consistency, we thus adopted the modified equation by Berman (1988), being the most representative of our dataset for both the temperature regimes (Figure 6, Table 6).

Within the hydrous expansion regime (303 - 748 K),  $a$ ,  $c$  and  $V$  expand almost linearly with increasing temperature by about 0.6, 1.3 and 2.5 %, respectively, with the following axial and volume thermal expansion coefficients:  $\alpha_{a(\text{hyd},303,1\text{bar})} = 1.16(3) \cdot 10^{-5} \text{ K}^{-1}$ ;  $\alpha_{c(\text{hyd},303,1\text{bar})} = 2.58(8) \cdot 10^{-5} \text{ K}^{-1}$ ;  $\alpha_{V(\text{hyd},303,1\text{bar})} = 4.88(8) \cdot 10^{-5} \text{ K}^{-1}$  (Table 6). The thermal expansion in cancrinite is more pronounced along [0001], which expands more than twice than on (0001) (Table 1, Figure 3). This anisotropic thermal expansion scheme is in perfect agreement with the high- $T$  data reported by Hassan (1996a) and Hassan et al. (2006), and with the low- $T$  data reported by Gatta et al. (2012).

At 748 K, the dehydration takes place, and the unit-cell edges accordingly decreased, reaching a relaxation only after 17,100 mins (about 12 days) (Table 2, Figure 4). Such a regime has been constantly monitored by measuring the unit-cell parameters as a function of time at constant temperature, shown in Figures 3 and 4. During such a contraction regime, the unit-cell volume undergoes a total reduction of 0.61%. In response to the loss of H<sub>2</sub>O, most of the volume contraction is accommodated along [0001] which, being the softest direction, undergoes the most pronounced shortening (*i.e.*, 0.41%) compared to that on (0001) (*i.e.*, 0.1% along  $a$ ) (Table 2, Figure 4). The anisotropy scheme is maintained during the whole dehydration process as shown in Figure 4.

At  $T > 748$  K, the unit-cell parameters of the quasi-anhydrous structure show further expansion with a rate similar to that of hydrated structure (Figure 3). The unit-cell volume expands by 0.44% between 748 and 823 K. The anisotropic expansion scheme of the quasi-anhydrous structure is similar to that observed for the hydrous cancrinite (*i.e.*  $\alpha_a < \alpha_c$ ), being  $c$  the direction with largest dilatation, with an expansion of 0.22% compared to 0.11% of the  $a$  edge in the temperature range between 748 and 823 K.

If we compare the Berman (1988) thermal equation of state fit for the hydrous (*i.e.*, 303 – 748 K) and quasi-anhydrous structures (*i.e.*, 748 – 823 K), the latter affected by higher uncertainty, we observe a significant difference (though not so pronounced) between the volume thermal expansion coefficients (*i.e.*,  $4.88(8) \cdot 10^{-5}$  and  $3.1(6) \cdot 10^{-5}$  K<sup>-1</sup>, Table 6). The fitting results provided in Table 6 confirm that the anisotropy scheme is maintained even when the dehydration process at 748 K is completed.

The unit-cell parameters were also measured at 773, 673, 573, 473, 373 and 291 K by cooling the crystal, using the same protocol applied for the increasing temperature ramp (longer times were needed to reach the structure relaxation). Unfortunately, a significant decrease in the intensity of the diffraction peaks coupled with a shape broadening, already observed at 823 K, suggested an irreversible reduction in crystallinity, likely due to the impending decomposition, which led to large uncertainties on the measured parameters. However, an inspection of the data reported in Table 1 and Figure 3 suggests that the dehydration process is an irreversible process at the time scale of the experiment.

- *High-temperature structural evolution and the effects of the dehydration process*

The structural model of our cancrinite at room conditions is consistent with those previously reported in the literature, and it is virtually identical to those obtained on crystals from the same locality (*i.e.*, Della Ventura et al. 2009; Gatta et al. 2012; Lotti et al. 2012). The framework is completely ordered with alternating SiO<sub>4</sub> and AlO<sub>4</sub> tetrahedra, as the Lowenstein's rule predicts and as observed in nearly all cancrinite-group minerals with Si:Al = 1:1. The columns of cages are filled with a Na<sup>+</sup> site (*i.e.*, Na1) in a special position on the 3-fold axis (Figure 1), almost at the same height of the S6R⊥[0001] oxygen atoms (Table 4), and H<sub>2</sub>O molecules (Ow, H<sub>2</sub>O-oxygen site) lying at the center of the cage in three symmetry-related and mutually exclusive split positions out of the axis (Figure 1, Table 4). The channel is stuffed with a single cationic site (*i.e.*, Na2/Ca2) near the walls and CO<sub>3</sub><sup>2-</sup> groups at the center, occupying two mutually exclusive iso-oriented configurations, both highly disordered along [0001] (Figures 1, 2, and 5; Table 4). The crystal chemical formula from the structure refinement is: [(Na<sub>5.30</sub>Ca<sub>0.70</sub>)(CO<sub>3</sub>)<sub>1.69</sub>][Na<sub>2</sub>(H<sub>2</sub>O)<sub>2</sub>][Al<sub>6</sub>Si<sub>6</sub>O<sub>24</sub>], which is in good agreement with the formula from the chemical analysis (Della Ventura et al. 2009).

The *sof*'s of the two independent CO<sub>3</sub><sup>2-</sup> groups, which were set free to vary in the HT-refinement, did not show any evident CO<sub>2</sub>-loss nor a redistribution between the sites with increasing temperature (Table 4). On the other hand, a test refinement suggested no significant loss of H<sub>2</sub>O at 448 K, consistent with the structure refinements of Hassan et al. (2006). The structure refinement at 748 K, based on intensity data collected when the dehydration process was completed, suggests that a minor amount of H<sub>2</sub>O molecules still persists within the cages, as shown by the difference-Fourier syntheses phased without the Ow site (Figure 5). The maps show weak maxima located at the Ow site, which hosts the H<sub>2</sub>O groups in the hydrous phase. The refinement of the Ow at 748 K, leaving both *sof* and *dp* free to vary was unstable. Consequently, the Ow *dp* was fixed to the value refined at 448 K and the *sof* set free to vary. With this strategy, the Ow *sof* refined to an occupancy of

5(1)% (*i.e.*, 0.30(6) H<sub>2</sub>O molecules *p.f.u*) (Table 4), which cannot be considered as a quantitative measure of the H<sub>2</sub>O content at 748 K (due to the bias induced by the fixed *dp*) but as a qualitative proof of a minor amount of H<sub>2</sub>O persistency after the dehydration process. The 748 K refinement also shows a strong elongation (along [0001]) of the Na1 anisotropic *dp* (Table 4dep), which suggest thermal and/or positional disorder of the Na<sup>+</sup> cations, no more coordinated along the *can* unit columns by the H<sub>2</sub>O molecules. It is worth noting that in the structure of a natural (almost) anhydrous cancrinite, found in small xenoliths in alkaline basalts of Laacher See (Eastern Eifel, Germany), the Na<sup>+</sup> site in the *can* units is split over three mutually exclusive positions along the 3-fold axis (Zubkova et al. 2011).

The loss of H<sub>2</sub>O at 748 K seems to influence only the Si-O2-Al inter-tetrahedral angle, as shown by the T-O-T *vs.* *T* evolution shown in Figure 7 and Table 5. The behavior of the T-O-T angles suggests that the dehydration affects predominantly the cages (*can* units), as shown in Figure 7, where cage- and channel-volumes *vs.* *T* are shown (Table 5). These values have been modeled following a protocol reported in other works on cancrinite-group minerals (*i.e.*, Lotti et al. 2012, 2014; Gatta et al. 2013): i)  $V_{ch} = \pi r^2 \cdot c$ , where  $V_{ch}$  is the channel volume,  $c$  is the length of the cell edge,  $r = (O1-O1 + O3-O4)/4$  and O1-O1 and O3-O4 are the symmetry-independent channel diameters (O1-O1 calculated as the projection onto (0001), Figure 1; Table 5); 2)  $V_{cg} = (V_{cell} - V_{ch})/2$ , where  $V_{cg}$  is the cage volume and  $V_{cell}$  the unit-cell volume.

The effects of the dehydration, manifested by the behavior of Si-O2-Al, can be described as a change in the tilting mechanism of the quasi-rigid (Si,Al)O<sub>4</sub> tetrahedra. This change can be followed through the evolution of several structural parameters of the *can* unit. The S6R $\perp$ [0001] ditrigonal rotation angle (Brigatti and Guggenheim 2002),  $\alpha_{S6R\perp[0001]} = 1/6 \cdot \sum_i |\theta_i - 120^\circ|/2$ , where  $\theta_i$  is the angle between the basal edges of the tetrahedra articulated in the 6-membered ring (Figure 1), first decreases (at 448 K) and then increases after the dehydration

(Table 5). The loss of H<sub>2</sub>O significantly affects the S4R units. The O3-O4 diameter (Figure 1) expands between 303 and 448 K, following the same, but opposite in sign, mechanism described at low-*T* (Gatta et al. 2012) and high-*P* (Lotti et al. 2012). At 748 K, we observe a shortening of this diameter (Table 5), as a consequence of the change in the tilting mechanism. The O3-O4<sub>S4R</sub> shortening likely governs the behavior of the cage volume,  $V_{cg}$ , between 448 and 748 K. This shortening is partially counterbalanced by the elongation of the O3-O4 diameter in the 12-ring channel, which is, on the contrary, almost constant between 303 and 448 K (Figure 1, Table 5), as also observed at low-*T* and high-*P*. The O1-O1 channel diameter seems not to be affected by the dehydration, as it shows a continuous increase with temperature (Table 5). The *T*-induced structural response along *c* is driven by the expansion of the double chains of tetrahedra, well described by the O3-O4-O3 angle (Figure 1, Table 5), which induces a hexagonalization of the S6R-windows (S6R $\angle$ [0001]) linking cages and channels (Figure 1). In this case, excluding the effects due to the shortening of the unit-cell *c* parameter in response to dehydration, no change in the deformation mechanisms is shown.

A structural mechanism, observed in the low-*T* and high-*P* behaviors of cancrinite, was the flattening of the cage, described by the closure of the O2-O2-O2 angle (Figure 1) in response to the contraction of the double chains of tetrahedra along [0001], coupled with the constant value of the (O2-O2)<sub>cw</sub> diameter referred to as “cage width” (dashed lines in Figure 1). This mechanism acts as a marker of the change of tetrahedra tilting. Between 303 and 448 K, we observe an opening of O2-O2-O2, due to the constant O2-O2 “cage width” (Table 5), but between 448 and 748 K a slight flattening of the cage occurs, despite the expansion along [0001], due to a strong increase of the O2-O2 (Table 5), which clearly marks a change in the framework deformation mechanisms.

Apparently, the channel-cations coordination environments do not seem to be affected by the dehydration process. An elongation of the shorter Na2/Ca2-O1, Na2/Ca2-O3' and Na2/Ca2-O4' and a shortening of the longer Na2/Ca2-O3'' and Na2/Ca2-O4'' bond lengths is observed (Figure 2, Table 5). An increase in both the average  $\langle \text{Na2/Ca2-O}_f \rangle$  and  $\langle \text{Na2/Ca2-O}_c \rangle$  bond lengths with the framework- and  $(\text{CO}_3^{2-})$ -oxygen atoms, respectively, is observed (Table 5).

The reasons for the change in the tilting mechanism can be inferred by following the evolution of the Na1 coordination environment. At room conditions, the  $\text{Na}^+$  cation is 8-fold bonded with four shorter lengths (to three O2 and one Ow) and four longer lengths (to three O1 and the other Ow) (Figure 2). At 448 K, we observe an increase in Na1-O2 and a decrease in Na1-O1 (Table 5), which is the same response, but opposite in sign, observed at low- $T$  and high- $P$  (Gatta et al. 2012; Lotti et al. 2012). At 748 K, despite the continuous decrease in Na1-O1, an inversion of the Na1-O2 vs.  $T$  behavior is shown (Table 5). Therefore, we can infer that in the hydrous 303 – 448 K range, not affected by  $\text{H}_2\text{O}$  loss, the cancrinite structural evolution is driven by the same mechanism (but opposite in sign) which drives the framework re-arrangement at low temperature (down to 100 K) and high pressure (up to 6.63 GPa). The change in the tilting mechanism, induced by dehydration, is likely driven by the tendency to minimize the Na1-O1 and Na1-O2 bond distances, in order to compensate the loss in the bond-valence contribution of the  $\text{H}_2\text{O}$  oxygen site, Ow.

The analysis of the equivalent/isotropic displacement parameters evolution with temperature (Table 4) shows an expected increase for all of them, but those related to the  $\text{CO}_3^{2-}$  groups. As already reported by a low- $T$  study of cancrinite from the same locality (Gatta et al. 2012), this is an indirect evidence for the strong positional disorder of the anionic groups along  $[0001]$ .

- *Comparison with previous studies*

Hassan (1996a) and Hassan et al. (2006) described the thermo-elastic behavior of cancrinite on the basis of *in-situ* powder diffraction data. A similar behavior can be deduced from our thermo-elastic parameters and those calculated on the basis of the data of Hassan et al. (2006), for the range 298-769 K, (*i.e.*,  $\alpha_r(303\text{K}, 1\text{bar}) = 4.7(8) \cdot 10^{-5} \text{ K}^{-1}$ ;  $\alpha_a(303\text{K}, 1\text{bar}) = 1.1(2) \cdot 10^{-5} \text{ K}^{-1}$ ;  $\alpha_c(303\text{K}, 1\text{bar}) = 2.4(5) \cdot 10^{-5} \text{ K}^{-1}$ ). However, our data about the dehydration process differ by those of Hassan (1996a, 1996b) and Hassan et al. (2006). Hassan (1996a, 1996b) and Hassan et al. (2006) set the heating rate as 60, 5 and 9.5 K/min, respectively. Sirbescu and Jenkins (1999) reported two comparative thermogravimetric analyses on a synthetic  $(\text{CO}_3^{2-})$ -cancrinite. In the first experiment, a computer-automated analysis, within the range 383-1623 K and a heating rate 2 K/min, was performed. For the second, a manual procedure was used with repeated weightings at each step until a constant weight was reached. The manual procedure required a period of 10 days, with an average heating rate of 0.06 K/min. Sirbescu and Jenkins (1999) reported a noticeable lower mass loss, at any given temperature, for the automated analysis. This was ascribed to the faster heating rate (*i.e.*, 2 K/min), concluding that such a rate did not allow sufficient time for the volatiles to diffuse out of the cancrinite crystals. A release of “zeolitic water” was reported within the range  $\sim 573$ -1058 K, with a dehydration rate that significantly decreases with increasing temperature (Sirbescu and Jenkins 1999). In our experiments, we increased temperature by steps of 25 K, with a dwell time of about 30 mins in order to achieve the structure relaxation. If we consider the slow mechanism of dehydration that we observed with our protocol, the heating rates adopted by Hassan (1996a, 1996b) and Hassan et al. (2006) appear to be too high, and so this might explain some differences on the dehydration process (Figure 8). Our experimental findings corroborate the results of Sirbescu and Jenkins (1999).

The protocol we used in this study was extremely useful to accurately bracket the dehydration- $T$  and shed lights on the actual rate of the dehydration, which, to our knowledge, had not been reported so far. In fact, as shown in Table 2, the process of dehydration at 748 K took approximately 12 days. Moreover, a more detailed description of the  $T$ - and dehydration-induced structural re-arrangement has been carried out, since this was lacking or was not the main topic in the works devoted to cancrinite behavior at high-temperature (Hassan 1996a, 1996b; Sirbescu and Jenkins 1999; Fechtelkord et al. 2001; Hassan et al. 2006; Isupova et al. 2010). It is interesting to point out some similar findings between our structural data and those from Fechtelkord et al. (2001) and Isupova et al. (2010). In particular: i) Fechtelkord et al. (2001) reported two structure refinements of a  $\text{NO}_3$ -cancrinite at room- $T$  and its partially dehydrated form at 673 K, showing a decrease of Na1-O1 and a constant Na1-O2; ii) an inversion of the Si-O2-Al *vs.*  $T$  behavior following the dehydration process was reported by Isupova et al. (2010), showing strong similarities with T-O-T *vs.*  $T$  behavior from our data (Table 5).

## ACKNOWLEDGEMENTS

The authors wish to thank Ross J. Angel for the new version of EoSFit software. GDG and PL acknowledge the Italian Ministry of Education, MIUR-Project: “Futuro in Ricerca 2012 - ImPACT- RBFR12CLQD”. FC acknowledges support by the University of Torino “Progetti di ricerca finanziati dall'Università degli Studi di Torino (ex 60%)” – year 2012. MA has been supported by the ERC starting grant # 307322 to FN. The Editor M. Rieder and two anonymous reviewers are thanked.

## REFERENCES

- Alvaro M, Cámara F, Domeneghetti M, Nestola F, and Tazzoli V (2011) HT P2<sub>1</sub>/c–C2/c phase transition and kinetics of Fe<sup>2+</sup>–Mg order–disorder of an Fe-poor pigeonite: implications for the cooling history of ureilites. *Contrib Mineral Petrol* 162:599-613.
- Berman RG (1988) Internally-Consistent Thermodynamic Data for Minerals in the System Na<sub>2</sub>O-K<sub>2</sub>O-CaO-MgO-FeO-Fe<sub>2</sub>O<sub>3</sub>-Al<sub>2</sub>O<sub>3</sub>-SiO<sub>2</sub>-TiO<sub>2</sub>-H<sub>2</sub>O-CO<sub>2</sub>. *J Petrol* 29:445-522.
- Bonaccorsi E, Merlino S (2005). Modular Microporous Minerals: Cancrinite-Davyne Group and C-S-H Phases. In: Ferraris G, Merlino S (eds) *Micro- and Mesoporous Mineral Phases, Reviews in Mineralogy and Geochemistry*. Vol. 57. Mineralogical Society of America and Geochemical Society, Washington DC, pp. 241-290.
- Brigatti MF, Guggenheim S (2002) Mica crystal chemistry and the influence of pressure, temperature, and solid solution on atomistic models. In: Mottana A, Sassi FP, Thompson JB, Guggenheim S (eds) *Micas: Crystal Chemistry and Metamorphic Petrology, Reviews in Mineralogy and Geochemistry*. Vol. 46. Mineralogical Society of America and Geochemical Society, Washington DC, pp. 1-98.
- Cámara F, Bellatreccia F, Della Ventura G, and Mottana A (2005) Farneseite, a new mineral of the cancrinite - sodalite group with a 14-layer stacking sequence. *Eur J Mineral* 17:839-846.
- Della Ventura G, Gatta GD, Redhammer GJ, Bellatreccia F, Loose A, Parodi GC (2009) Single-crystal polarized FTIR spectroscopy and neutron diffraction refinement of cancrinite. *Phys Chem Mineral* 36:193-206.
- Farrugia LJ (1999) WinGX suite for small-molecule single-crystal crystallography. *J Appl Crystallogr* 32:837-838.

Fechtelkord M, Stief F, Buhl JC (2001) Sodium cation dynamics in nitrate cancrinite: A low and high temperature  $^{23}\text{Na}$  and  $^1\text{H}$  MAS NMR study and high temperature Rietveld structure refinement. *Am Mineral* 86:165-175.

Ferrari S, Nestola F, Massironi M, Maturilli A, Helbert J, Alvaro M, Domeneghetti MC, Zorzi F (2014) In-situ high-temperature emissivity spectra and thermal expansion of *C2/c* pyroxenes: implications for the surface of Mercury. *Am Mineral* (*in press*, DOI: 10.2138/am.2014.9698)

Gatta GD, Lotti P, Kahlenberg V, Haefeker U (2012). The low-temperature behaviour of cancrinite: an in situ single-crystal X-ray diffraction study. *Mineral Mag* 76:933-948.

Gatta GD, Lotti P, Kahlenberg V (2013) The low-temperature behavior of balliranoite (CAN topology): an in-situ single-crystal X-ray diffraction study. *Micropor Mesopor Mater* 174:44-53.

Grundy HD, Hassan I (1982) The crystal structure of a carbonate-rich cancrinite. *Can Mineral* 20:239-251.

Gottschalk M (1997) Internally consistent thermodynamic data for rock-forming minerals in the system  $\text{SiO}_2\text{-TiO}_2\text{-Al}_2\text{O}_3\text{-CaO-MgO-FeO-K}_2\text{O-Na}_2\text{O-H}_2\text{O-CO}_2$ . *Eur J Mineral* 9:175-223.

Hassan I (1996a) Thermal expansion of cancrinite. *Mineral Mag* 60:949-956.

Hassan I (1996b) The thermal behavior of cancrinite. *Can Mineral* 34:893-900.

Hassan I, Grundy HD (1991) The crystal structure of basic cancrinite, ideally  $\text{Na}_8[\text{Al}_6\text{Si}_6\text{O}_{24}](\text{OH}_2)\cdot 3\text{H}_2\text{O}$ . *Can Mineral* 29:377-383.

Hassan I, Antao SM, Parise JB (2006) Cancrinite: Crystal structure, phase transitions, and dehydration behavior with temperature. *Am Mineral* 91:1117-1124.

Holland TJB, Powell R (1998) An internally consistent thermodynamic data set for phases of petrological interest. *J Metamorph Geol* 16:309-343.

Isupova D, Ida A, Kihara K, Morishita T, Bulka G (2010) Asymmetric thermal vibrations of atoms and pyroelectricity in cancrinite. *J Miner Petrol Sci* 105:29-41.

Kurdakova SV, Grishchenko RO, Druzhinina AI, Ogorodova LP (2013) Thermodynamic properties of synthetic calcium-free carbonate cancrinite. *Phys Chem Minerals* (*in press*, DOI 10.1007/s00269-013-0625-1).

Lehmann MS, Larsen FK (1974) A method for location of the peaks in step-scan measured Bragg reflexions. *Acta Crystallogr A* 30:580-584.

Lotti P, Gatta GD, Rotiroti N, Cámara F (2012) High-pressure study of a natural cancrinite. *Am Mineral* 97:872-882.

Lotti P, Gatta GD, Rotiroti N, Cámara F, Harlow GE (2014) The high-pressure behavior of balliranoite: a cancrinite-group mineral. *Z Kristallogr* (*in press*, DOI: 10.1515/zkri-2014-1626).

North ACT, Phillips DC, Mathews FS (1968) A semi-empirical method of absorption correction. *Acta Crystallogr A* 24:351-359.

Pawley AR, Redfern SAT, Holland TJB (1996) Volume behavior of hydrous minerals at high pressure and temperature: I. Thermal expansion of lawsonite, zoisite, clinozoisite, and diaspore. *Am Mineral* 81:335-340.

Pekov IV, Olysyh LV, Chukanov NV, Zubkova NV, Pushcharovsky DY (2011) Crystal chemistry of cancrinite-group minerals with an AB type framework: a review and new data. I. Chemical and structural variations. *Can Mineral* 49:1129-1150.

Poborchii VV (1994) Structure of one-dimensional selenium chains in zeolite channels by polarized Raman scattering. *J Phys Chem Solids* 55:737-743.

Poborchii VV, Lindner GG, Sato M (2002) Selenium dimers and linear chains in one-dimensional cancrinite nanochannels: Structure, dynamics, and optical properties. *J Chem Phys* 116:2609-2617

Redhammer GJ, Cámara F, Alvaro M, Nestola F, Tippelt G, Prinz S, Simons J, Roth G, and Amthauer G (2010) Thermal expansion and high-temperature  $P2_1/c-C2/c$  phase transition in clinopyroxene-type  $\text{LiFeGe}_2\text{O}_6$  and comparison to  $\text{NaFe}(\text{Si,Ge})_2\text{O}_6$ . *Phys Chem Mineral* 37:685-704.

Sheldrick GM (1997) SHELX-97. A Program for crystal structure refinement. University of Goettingen, Goettingen.

Sheldrick GM (2008) A short history of SHELX. *Acta Crystallogr A* 64:112-122.

Sirbescu M, Jenkins DM (1999) Experiments on the stability of cancrinite in the system  $\text{Na}_2\text{O}-\text{CaO}-\text{Al}_2\text{O}_3-\text{SiO}_2-\text{CO}_2-\text{H}_2\text{O}$ . *Am Mineral* 84:1850-1860.

Wilson AJC, Prince E (1999) International Tables for Crystallography. Volume C: Mathematical, Physical and Chemical Tables, second edn, Kluwer, Dordrecht.

Zubkova NV, Chukanov NV, Pekov IV, Pushcharovsky DY (2011). Low-Hydrous Cancrinite: Atomic Structure and Indicative Importance. *Dokl Earth Sci* 439:998-1001.

**Table 1.** Unit-cell parameters of cancrinite with temperature.

$T$ (K)	$a$ (Å)	$c$ (Å)	$V$ (Å <sup>3</sup> )
291*	12.6207(3)	5.1260(1)	707.10(3)
303	12.6251(4)	5.1249(1)	707.43(4)
303	12.6243(4)	5.1260(1)	707.50(4)
323	12.6279(4)	5.1282(1)	708.20(4)
348	12.6310(4)	5.1317(2)	709.03(4)
373	12.6345(5)	5.1354(1)	709.93(5)
398	12.6378(5)	5.1398(1)	710.92(4)
423	12.6426(4)	5.1435(1)	711.97(4)
448	12.6454(6)	5.1468(2)	712.74(5)
473	12.6480(5)	5.1504(1)	713.54(5)
473	12.6485(5)	5.1501(2)	713.55(5)
498	12.6530(6)	5.1540(2)	714.61(6)
498	12.6525(6)	5.1545(2)	714.61(6)
498	12.6524(4)	5.1537(1)	714.49(4)
523	12.6564(6)	5.1578(2)	715.51(6)
548	12.6614(6)	5.1623(2)	716.70(6)
573	12.6647(4)	5.1658(2)	717.55(4)
598	12.6699(5)	5.1700(2)	718.73(5)
623	12.6737(5)	5.1742(2)	719.75(5)
648	12.6771(5)	5.1793(2)	720.84(5)
673	12.6817(6)	5.1829(2)	721.87(5)
698	12.6867(5)	5.1873(2)	723.06(5)
723	12.6909(5)	5.1915(1)	724.12(4)
748	12.6942(6)	5.1931(3)	724.72(6)
748 <sup>†</sup>	12.6814(6)	5.1720(2)	720.32(6)
773 <sup>†</sup>	12.6850(10)	5.1761(2)	721.29(9)
773 <sup>†</sup>	12.6848(4)	5.1755(2)	721.19(4)
798 <sup>†</sup>	12.6914(5)	5.1791(2)	722.44(5)
823 <sup>†</sup>	12.6957(5)	5.1833(2)	723.52(5)
773 <sup>**</sup>	12.690(1)	5.174(4)	721.6(6)
673 <sup>**</sup>	12.658(8)	5.168(8)	717.1(1.3)
573 <sup>**</sup>	12.658(4)	5.154(11)	715.2(1.5)
473 <sup>**</sup>	12.645(9)	5.140(14)	711.7(2.1)
373 <sup>**</sup>	12.626(4)	5.123(5)	707.4(8)
291 <sup>**</sup>	12.611(6)	5.118(10)	705.0(1.4)

*Note:* At 303, 473, 498, 773, the cell parameters were measured more than one time; \*data collected with the crystal in air (no furnace, no silica vial), <sup>†</sup>data collected after the dehydration process, \*\* data collected during temperature decrease.

**Table 2.** Unit-cell parameters of cancrinite with time at 748 K.

Time (min)	$a$ (Å)	$c$ (Å)	$V$ (Å <sup>3</sup> )
0	12.6942(6)	5.1931(3)	724.72(6)
131	12.6942(6)	5.1928(3)	724.67(6)
254	12.6933(5)	5.1927(2)	724.56(5)
334	12.6933(5)	5.1927(2)	724.56(5)
488	12.6933(7)	5.1913(3)	724.36(7)
1270	12.6933(5)	5.1910(2)	724.33(5)
1378	12.6935(5)	5.1897(3)	724.15(6)
1570	12.6907(5)	5.1894(2)	723.80(5)
1692	12.6911(5)	5.1886(3)	723.73(6)
2912	12.6870(6)	5.1817(3)	722.30(6)
3210	12.6870(4)	5.1815(2)	722.28(5)
3391	12.6869(5)	5.1812(3)	722.23(5)
3601	12.6868(4)	5.1807(2)	722.14(5)
4536	12.6871(6)	5.1798(3)	722.06(7)
5782	12.6860(6)	5.1791(3)	721.82(6)
5931	12.6851(5)	5.1782(3)	721.61(6)
6337	12.6843(10)	5.1779(2)	721.47(8)
6337	12.6857(5)	5.1779(2)	721.63(5)
6419	12.6825(9)	5.1775(2)	721.22(7)
6419	12.6849(5)	5.1774(2)	721.47(5)
12099	12.6849(5)	5.1774(2)	721.47(5)
15000	12.6824(1)	5.1786(8)	721.35(11)
15180	12.6820(5)	5.1730(2)	720.52(5)
15360	12.6812(5)	5.1727(2)	720.39(5)
15540	12.6807(6)	5.1726(2)	720.32(6)
15720	12.6814(6)	5.1726(2)	720.39(6)
15900	12.6798(5)	5.1718(2)	720.11(5)
16080	12.6787(5)	5.1722(2)	720.05(6)
16260	12.6822(5)	5.1727(2)	720.50(5)
16440	12.6801(5)	5.1725(2)	720.23(4)
16620	12.6812(5)	5.1726(2)	720.37(5)
16800	12.6821(5)	5.1723(2)	720.44(5)
16980	12.6803(6)	5.1718(2)	720.16(5)
17100	12.6814(6)	5.1720(2)	720.32(6)

**Table 3.** Details pertaining to the data collection protocol and structure refinements at different temperatures

$T$ (K)	303 ( $T_0$ )	478 ( $T_i$ )	748 ( $T_2$ )
$a$ (Å)	12.6261(4)	12.6554(5)	12.6849(5)
$c$ (Å)	5.1257(2)	5.1468(1)	5.1774(2)
$V$ (Å <sup>3</sup> )	707.66(4)	712.74(4)	721.47(5)
Maximum $2\theta$ (°)	59.90	59.97	59.88
	$0 \leq h \leq 11$	$0 \leq h \leq 12$	$0 \leq h \leq 11$
	$-17 \leq k \leq 15$	$-17 \leq k \leq 14$	$-17 \leq k \leq 14$
	$-7 \leq l \leq 7$	$-7 \leq l \leq 7$	$-7 \leq l \leq 7$
Measured reflections	3408	3542	3470
Unique reflections	1366	1385	1393
Unique reflections with $F_0 > 4\sigma(F_0)$	1057	1003	949
$R_{\text{int}}$	0.0696	0.0718	0.0679
Number of l.s. parameters	90	84	84
$R_1, F_0 > 4\sigma(F_0)$	0.0525	0.0567	0.0596
$R_1$ , all data	0.0743	0.0905	0.1016
$wR_2$	0.1330	0.1436	0.1587
GooF	1.017	1.093	1.030
Residuals ( $e\text{Å}^{-3}$ )	+0.64/-0.53	+1.09/-0.54	+0.85/-0.47
<p>Note: <math>R_{\text{int}} = \Sigma  F_{\text{obs}}^2 - (\text{mean})  / \Sigma [F_{\text{obs}}^2]</math>; <math>R_1 = \Sigma   F_{\text{obs}}  -  F_{\text{calc}}   / \Sigma  F_{\text{obs}} </math>; <math>wR_2 = \{\Sigma [w(F_{\text{obs}}^2 - F_{\text{calc}}^2)^2] / \Sigma [w(F_{\text{obs}}^2)^2]\}^{0.5}</math>, <math>w = 1 / [\sigma^2(F_{\text{obs}}^2) + (0.01 \cdot P)^2]</math>, <math>P = [\text{Max}(F_{\text{obs}}^2, 0) + 2 \cdot F_{\text{calc}}^2] / 3</math>.</p>			

**Table 4.** Atomic fractional coordinates, site occupancy factors (*s.o.f.*) and isotropic/equivalent displacement parameters ( $\text{\AA}^2$ ) at different temperatures.

Atom site	<i>T</i> (K)	Occupancy	<i>x</i>	<i>y</i>	<i>z</i>	$U_{\text{eq}}/U_{\text{iso}}$
Si	303	1.0	0.32814(9)	0.41065(9)	0.7019(8)	0.0079(2)
	478	1.0	0.3284(1)	0.4108(1)	0.6945(4)	0.0107(2)
	748	1.0	0.3286(1)	0.4119(1)	0.7304(4)	0.0163(3)
Al	303	1.0	0.0754(1)	0.4124(1)	0.7027(8)	0.0081(2)
	478	1.0	0.0748(1)	0.4121 (1)	0.6952(4)	0.0106(2)
	748	1.0	0.0747(1)	0.4133(1)	0.7319(4)	0.0165(3)
O1	303	1.0	0.2038(3)	0.4052(3)	0.611(1)	0.0159(7)
	478	1.0	0.2040(2)	0.4064(3)	0.6089(7)	0.0199(7)
	748	1.0	0.2047(3)	0.4083(4)	0.6516(8)	0.032(1)
O2	303	1.0	0.1147(3)	0.5641(3)	0.679(1)	0.0205(7)
	478	1.0	0.1133(3)	0.5630(2)	0.6720(8)	0.0249(7)
	748	1.0	0.1157(4)	0.5641(3)	0.710(1)	0.038(1)
O3	303	1.0	0.0303(3)	0.3508(3)	0.013(1)	0.0147(7)
	478	1.0	0.0286(3)	0.3496(3)	0.0033(6)	0.0197(7)
	748	1.0	0.0247(4)	0.3483(4)	0.0331(8)	0.029(1)
O4	303	1.0	0.3142(3)	0.3585(3)	-0.005(1)	0.0144(6)
	478	1.0	0.3144(3)	0.3567(3)	-0.0143(6)	0.0192(7)
	748	1.0	0.3174(4)	0.3562(4)	0.0164(7)	0.0290(9)
Na1	303	1.0	2/3	1/3	0.088(1)	0.035(1)
	478	1.0	2/3	1/3	0.081(1)	0.048(1)
	748	1.0	2/3	1/3	0.111(2)	0.071(2)
Ow	303	1.0	0.315(2)	0.699(2)	0.137(4)	0.062(5)
	478	1.0	0.312(2)	0.697(2)	0.142 (4)	0.082(6)
	748	1.0	0.286(13)	0.696(13)	0.20(5)	0.082
Na2/Ca2	303	Na, 0.88(1) Ca, 0.12(1)	0.1232(2)	0.2499(2)	0.2451(9)	0.0265(7)
	478	“	0.1233(2)	0.2500(2)	0.2377(5)	0.0355(5)
	748	“	0.1240(2)	0.2516(3)	0.2693(7)	0.0554(8)
C1	303	0.37(1)	0	0	0.358(5)	0.044(5)
	478	0.351(9)	0	0	0.309(4)	0.042(3)
	748	0.36(1)	0	0	0.415(5)	0.035(4)
OC1	303	0.37(1)	0.1189(4)	0.061(1)	0.351(5)	0.059(4)

	478	0.351(9)	0.1175(4)	0.058(1)	0.347(2)	0.044(2)
	748	0.36(1)	0.1175(5)	0.062(2)	0.394(4)	0.069(4)
C2	303	0.47(1)	0	0	0.113(6)	0.044(5)
	478	0.451(9)	0	0	0.099(4)	0.042(3)
	748	0.46(1)	0	0	0.142(5)	0.035(4)
OC2	303	0.47(1)	0.1191(4)	0.061(1)	0.125(4)	0.059(4)
	478	0.451(9)	0.1183(4)	0.0623(9)	0.128(2)	0.044(2)
	748	0.46(1)	0.1179(5)	0.061(1)	0.161(3)	0.069(4)

---

**Table 5.** Relevant bond distances (Å), diameters (Å), angles (°), ditrigonal rotation angle  $\alpha$  (°) of the  $S6R\perp[0001]$ , and cage/channel-volumes (Å<sup>3</sup>) at different temperatures.

	$T$ (K)	303 ( $T_0$ )	478 ( $T_1$ )	748 ( $T_2$ )
Si-	O1	1.605(3)	1.607(3)	1.603(4)
	O2	1.608(3)	1.608(3)	1.610(4)
	O3	1.626(3)	1.624(3)	1.624(4)
	O4	1.614(3)	1.620(3)	1.616(4)
	<Si-O>	1.613(3)	1.615(3)	1.613(4)
Al-	O1	1.734(3)	1.730(3)	1.732(4)
	O2	1.726(3)	1.722(3)	1.717(4)
	O3	1.735(3)	1.737(3)	1.730(4)
	O4	1.756(3)	1.747(3)	1.746(4)
	<Al-O>	1.738(3)	1.734(3)	1.731(4)
	Si-O1-Al	147.2(2)	148.0(2)	151.2(3)
	Si-O2-Al	151.2(2)	152.5(2)	151.0(3)
	Si-O3-Al	133.4(2)	134.0(2)	136.1(3)
	Si-O4-Al	133.3(2)	134.1(2)	136.6(3)
Na1-	O1(x3)	2.862(3)	2.854(2)	2.846(3)
	O2(x3)	2.437(4)	2.455(3)	2.446(4)
	Ow'	2.38(2)	2.33(2)	2.3(2)
	Ow''	2.87(2)	2.94(2)	3.2(3)
Na2/Ca2	O1	2.532(6)	2.566(4)	2.623(6)
	O3'	2.432(6)	2.446(5)	2.476(7)
	O3''	2.893(5)	2.880(4)	2.863(6)
	O4'	2.456(5)	2.466(4)	2.498(5)
	O4''	2.914(6)	2.895(5)	2.885(7)
	OC1'	2.418(17)	2.421(8)	2.44(2)
	OC1''	2.456(14)	2.439(11)	2.45(2)
	OC1'''	2.48(2)	2.514(12)	2.48(2)
	OC2'	2.416(18)	2.409(12)	2.449(18)
	OC2''	2.440(14)	2.474(9)	2.504(16)
	OC2'''	2.451(9)	2.467(7)	2.471(11)
	<Na2/Ca2-O <sub>fr</sub> >	2.645(6)	2.651(4)	2.669(6)
	<Na2/Ca2-O <sub>CO3</sub> >	2.441(15)	2.451(10)	2.471(16)
	C1-OC1	1.301(5)	1.302(5)	1.296(6)
	C2-OC2	1.304(5)	1.305(5)	1.299(6)
	(O2-O2) <sub>cw</sub>	8.487(6)	8.473(5)	8.545(7)
	O2-O2-O2	91.1(2)	92.0(1)	90.9(2)
	(O1-O1) <sub>ch</sub>	8.862(5)	8.901(5)	8.971(7)
	(O3-O4) <sub>ch</sub>	8.487(4)	8.485(4)	8.536(5)
	(O3-O4) <sub>S4R</sub>	4.145(6)	4.166(6)	4.155(8)
	O3-O4-O3	144.6(3)	146.39(16)	149.8(2)
	$\alpha_{S6R\perp[0001]}$	8.48(9)	7.99(8)	8.19(12)
	$V_{cg}$	202.4(2)	203.8(2)	204.9(3)
	$V_{ch}$	302.9(3)	305.2(3)	311.6(5)

*Note:* *fr* stands for framework, *cw* for cage width, *ch* for channel, *cg* for cage

**Table 6.** Results of the thermal equation of state fits based on the unit-cell parameters of this study. The EoSFit software was used (courtesy of RJ Angel). Further details are given in the text.

	<b>Volume</b>	<b><i>a</i>-axis</b>	<b><i>c</i>-axis</b>
Pawley et al. (1996), $T < 478\text{K}$			
$l_0(\text{\AA}), V_0(\text{\AA}^3)$	707.51(5)	12.6237(5)	5.1265(4)
$\alpha_{303,1\text{bar}}(\text{K}^{-1})$	$4.6(2) \cdot 10^{-5}$	$1.14(7) \cdot 10^{-5}$	$2.5(1) \cdot 10^{-5}$
$a_0(\text{K}^{-1})$	$8.63(4) \cdot 10^{-5}$	$1.7(1) \cdot 10^{-5}$	$5.2(3) \cdot 10^{-5}$
$a_1(\text{K}^{-1/2})$	$-1.7(5) \cdot 10^{-5}$	$-0.7(2) \cdot 10^{-4}$	$-2.7(6) \cdot 10^{-4}$
Berman (1988), $T < 478\text{K}$			
$l_0(\text{\AA}), V_0(\text{\AA}^3)$	707.50(5)	12.6237(3)	5.1264(3)
$\alpha_{303,1\text{bar}} = a_0(\text{K}^{-1})$	$4.88(8) \cdot 10^{-5}$	$1.16(3) \cdot 10^{-5}$	$2.58(8) \cdot 10^{-5}$
$a_1(\text{K}^{-1})$	$3.2(4) \cdot 10^{-8}$	$4.9(8) \cdot 10^{-9}$	$2.3(3) \cdot 10^{-9}$
Berman (1988), $T > 478\text{K}$			
$l_0(\text{\AA}), V_0(\text{\AA}^3)$	705.5 (1.0)	12.618(9)	5.116(6)
$\alpha_{303,1\text{bar}} = a_0(\text{K}^{-1})$	$3.1(6) \cdot 10^{-5}$	$0.6(3) \cdot 10^{-5}$	$1.9(5) \cdot 10^{-5}$
$a_1(\text{K}^{-1})$	$6.4(1.4) \cdot 10^{-8}$	$2.1(9) \cdot 10^{-9}$	$2.1(1.0) \cdot 10^{-9}$

**Figure 1.** (*Left side*) The [CAN]-framework viewed down [0001]. Six *can* units columns surround a 12-ring channel. The columns are occupied by  $\text{Na}^+\text{-H}_2\text{O-Na}^+\text{-H}_2\text{O}$  chains, where the Ow occupies three mutually exclusive positions out of the 3-fold axis. The channel is stuffed by  $\text{Na}^+/\text{Ca}^{2+}$  sites near the walls and  $\text{CO}_3^{2-}$  groups in the center. Large purple spheres:  $\text{Na}^+/\text{Ca}^{2+}$  sites; smaller red spheres:  $\text{H}_2\text{O}$  oxygen; black smaller spheres: C site. (*Right side*) Two base-sharing *can* units.

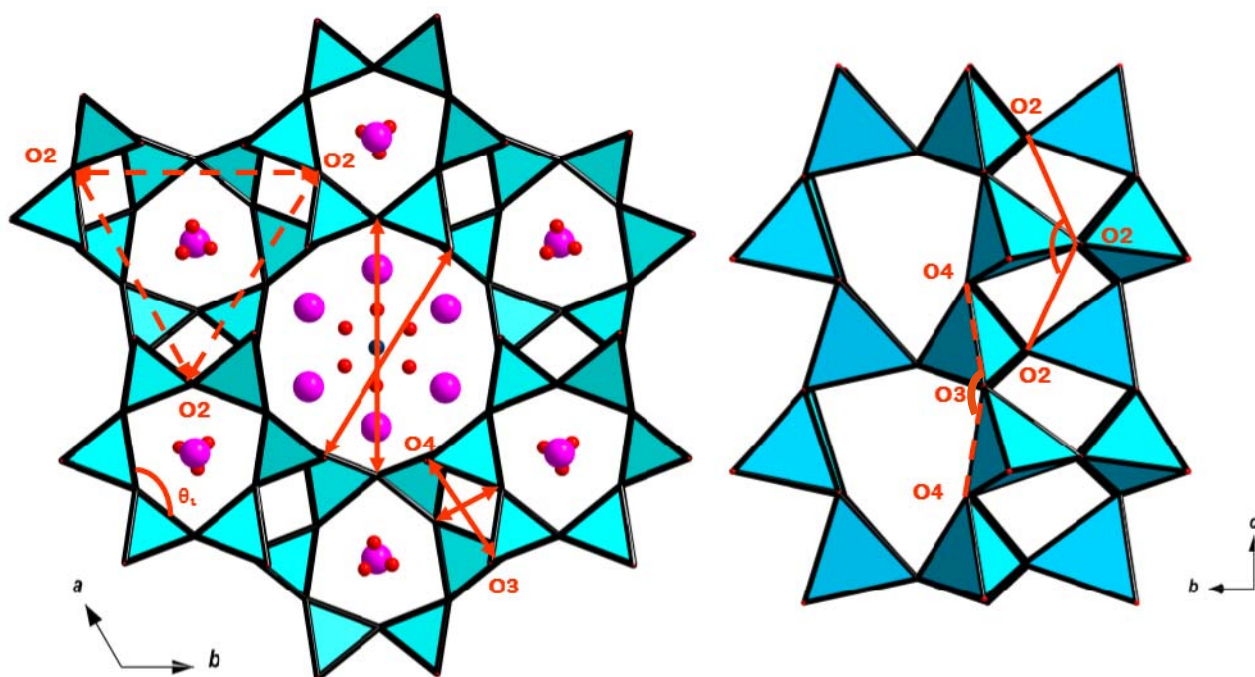


**Figure 2.** (*Left*) The  $\text{Na}^+$  coordination environment within the *can* units columns. Na1 is bonded to the framework oxygen atoms through three shorter Na1-O2 and three longer Na1-O1 bond lengths. The  $\text{Na}^+$ -H<sub>2</sub>O chains are made by a shorter Na1-Ow' and a longer Na1-Ow'' bonds. (*Right*) The  $\text{Na}^+/\text{Ca}^{2+}$  coordination environment within the channels. The cation at the Na2/Ca2 site is bonded to five framework oxygen atoms on a side and up to three carbonate oxygen atoms on the other side, with several possible configurations (see Della Ventura et al. 2009, for a comprehensive description).

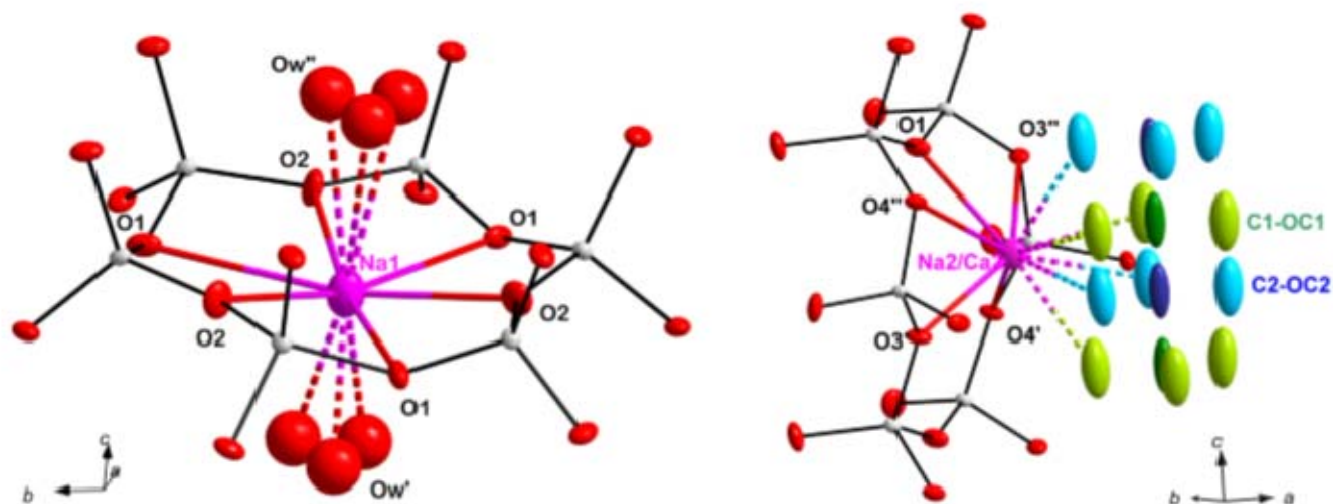


**Figure 3.** The evolution of the unit-cell parameters as a function of temperature. Full symbols represent data collected increasing- $T$ , open symbols represent data collected during the cooling.

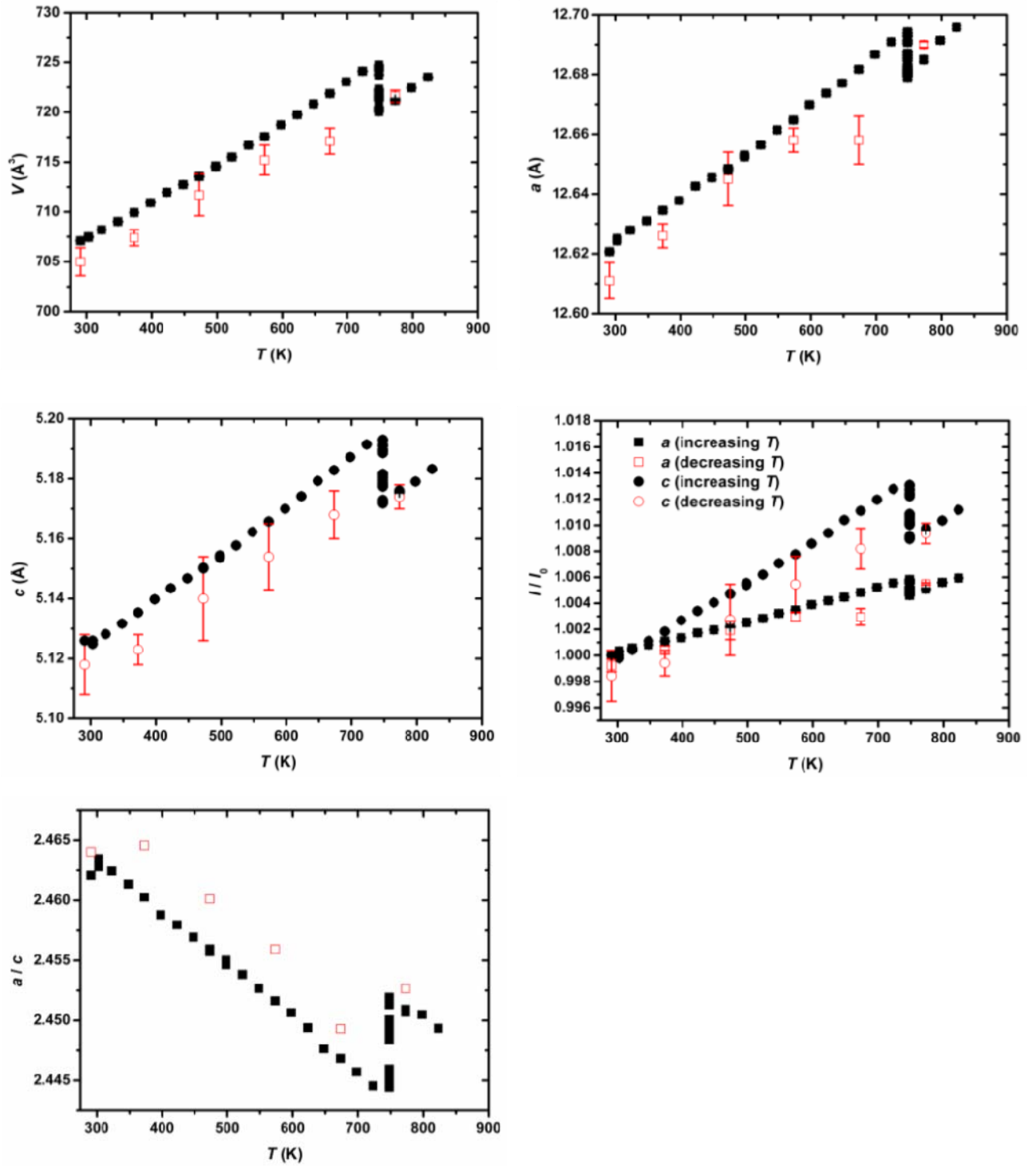


**Figure 4.** Variations of unit-cell volume,  $a/a_0$  and  $c/c_0$ , and  $a/c$  ratio with increasing time at constant temperature (748 K). The e.s.d.'s are smaller than the symbols.

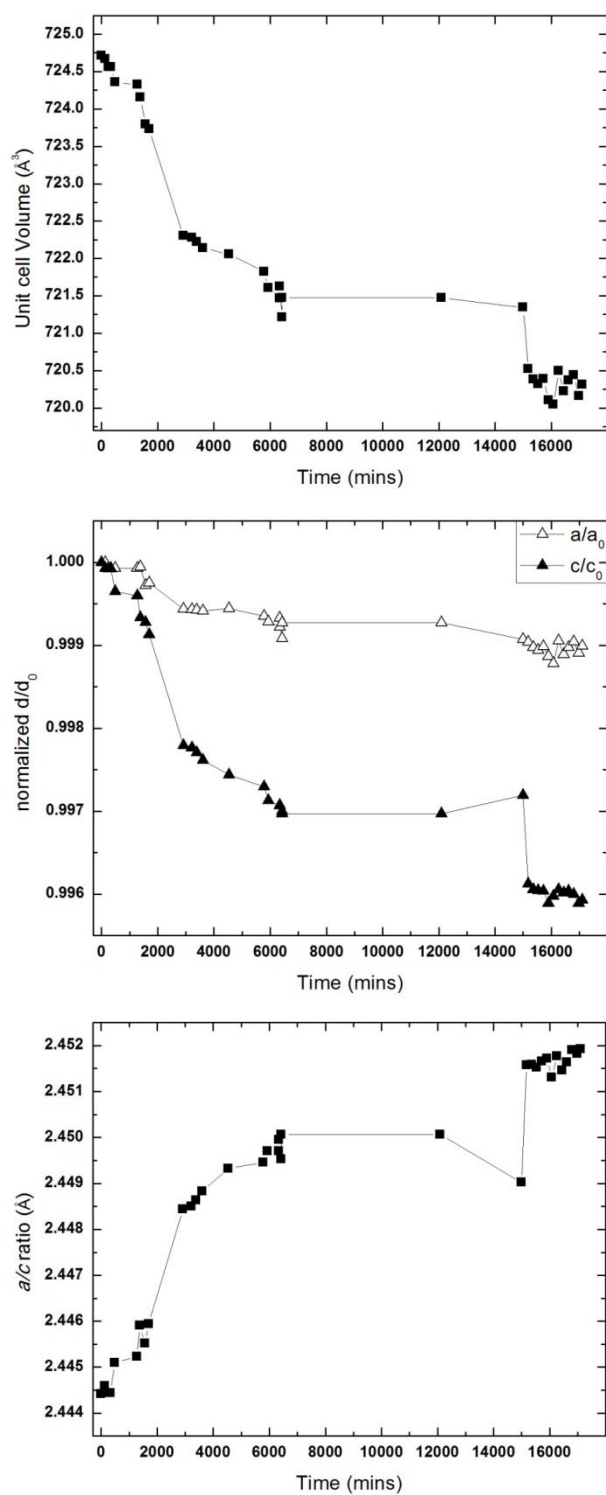


**Figure 5.** (*Top*) Difference-Fourier map of electron density phased without the  $\text{CO}_3^{2-}$  groups at  $T = 303$  K;  $0 < c < 1$ ,  $-0.2 < x < 0.2$ . (*Bottom*) Difference-Fourier map of electron density phased without the Ow sites at  $T = 748$  K, showing the *can* unit content in a plane parallel to (0001) at  $z = 0.20$  ( $\text{H}_2\text{O}$  molecules).

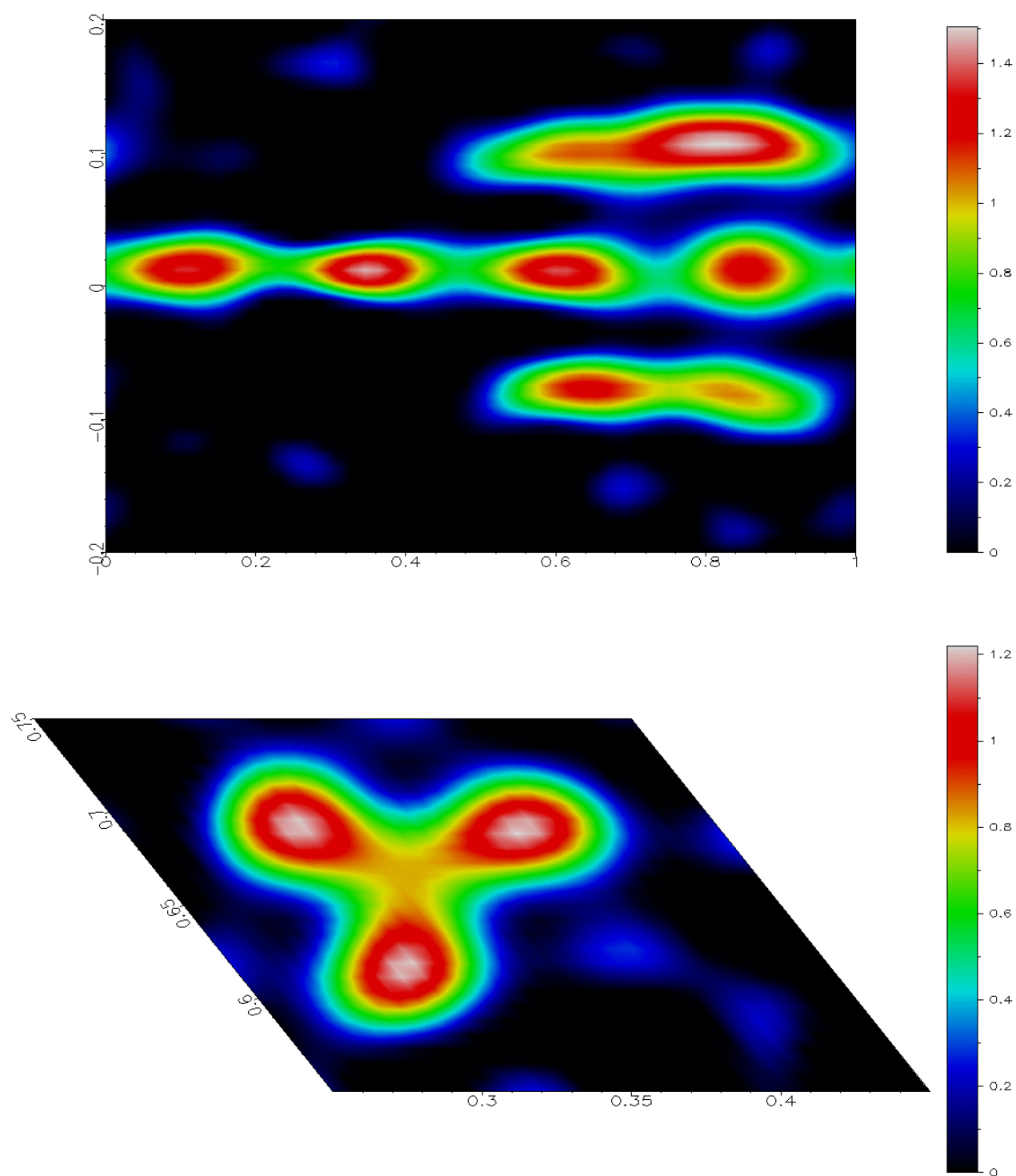


**Figure 6.** Difference between experimental and calculated volume (by thermal equation of state fit),  $\delta V$ , as a function of temperature. The  $\delta V$  clearly shows that both the modified equations of Pawley et al. (1996) and Berman (1988) reproduce very well the thermal expansion behavior from room- $T$  to 748 K, with the exception of the last data points due to the impending dehydration (arrow). The grey area represents the average  $\delta V$  *e.s.d.* deduced on the basis of the experimental and calculated  $V$  *e.s.d.*.

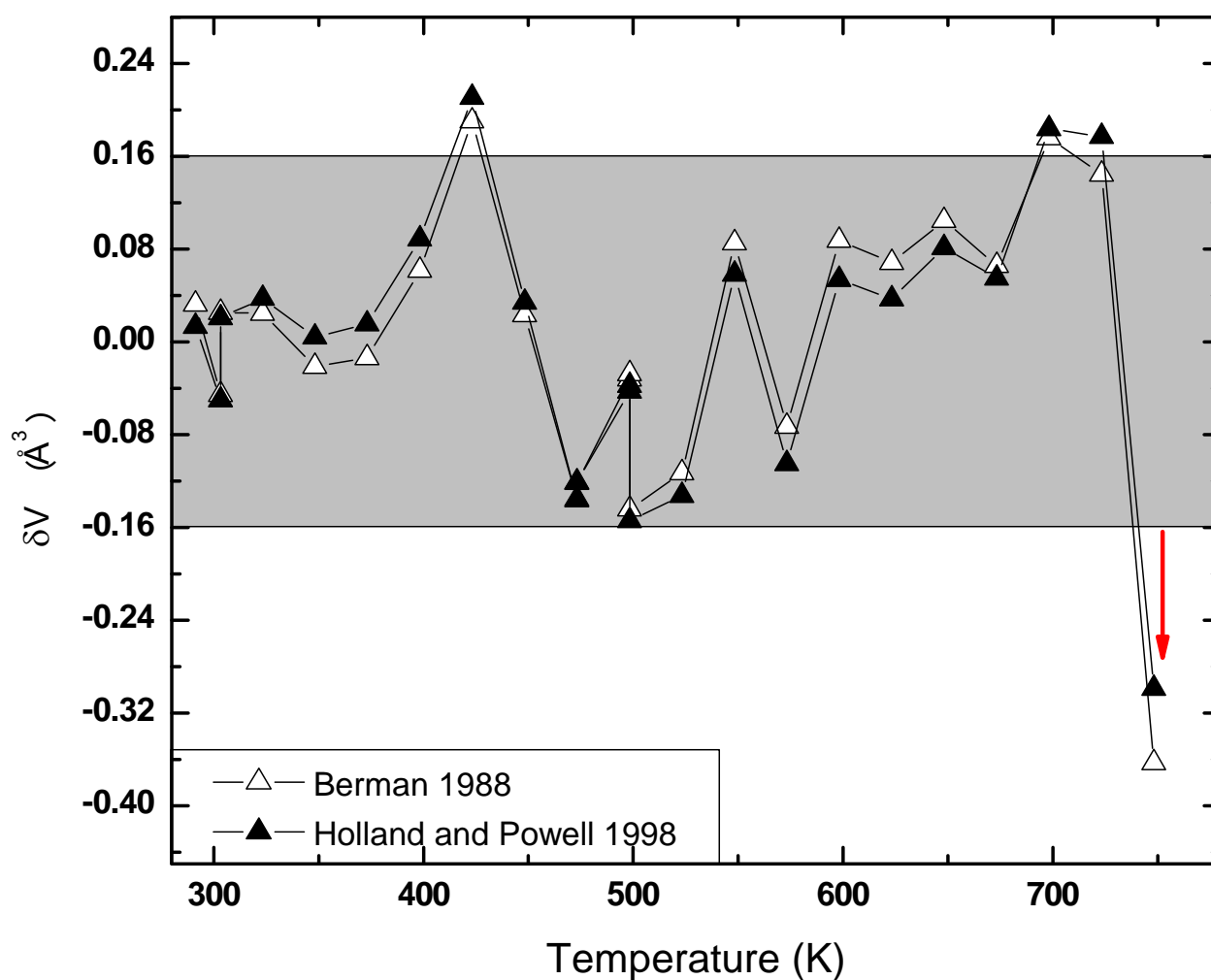


**Figure 7.** (Top) Evolution of the Si-O-Al intertetrahedral angles (normalized to the values at 303 K) with  $T$ . (Bottom) Variation with  $T$  of the channel ( $V_{ch}$ ) and *can* unit ( $V_{cg}$ ) volumes.

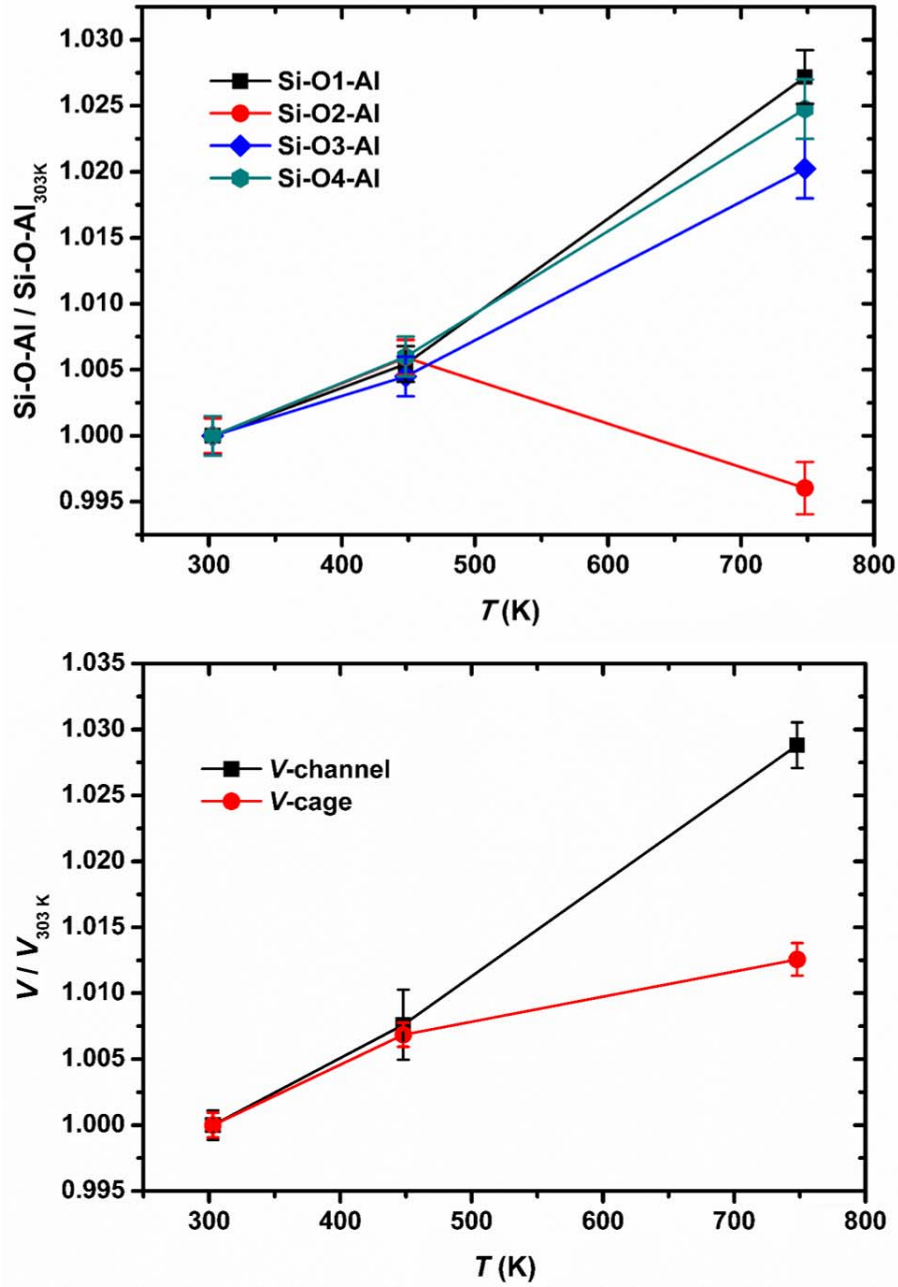


**Figure 8.** Unit-cell volume as a function of  $T$ . Comparison of our data with those by Hassan et al. (2006) and Hassan (1996a).

